INTERNATIONAL JOURNAL FOR NUMERICAL METHODS IN FLUIDS, VOL. 19, 849–863 (1994)

AN UNSTRUCTURED GRID ALGORITHM FOR THE SOLUTION OF MAXWELL'S EQUATIONS IN THE TIME DOMAIN

K. MORGAN

Department of Civil Engineering, University of Wales, Swansea SA2 8PP, U.K.

O. HASSAN

CDR, Innovation Centre, University of Wales, Swansea SA2 8PP, U.K.

AND

J. PERAIRE

Department of Aeronautics and Astronautics, MIT, Cambridge, MA 02139, U.S.A.

SUMMARY

The solution of problems involving the scattering of plane electromagnetic waves by perfectly conducting obstacles is considered. The governing equations are Maxwell's equations, which are expressed in a conservation form. The solution is then obtained by modifying a technique which was applied originally to the solution of the compressible Euler equations on a mesh consisting of an unstructured assembly of linear triangular elements in 2D or linear tetrahedral elements in 3D. The computed solution can be used to determine the radar cross-section of the scatterer.

KEY WORDS Unstructured grids Electromagnetic scattering Time domain method

1. INTRODUCTION

Computational electromagnetics has been identified as a key technology for allowing advances in aerospace design. The development of suitable computational tools in this area is essential if stringent design requirements, such as low observability are to be met. In recent years the time domain method of solution of Maxwell's equations has been developed as an alternative to the more traditional method-of-moments approach. The interest in the time domain method has been driven by the expectation that its reduced computational requirements should permit the modelling of the large problems which are of current industrial interest.[1]

A popular time domain approach for the solution of Maxwell's equations is the method due to Yee,[2] which is basically a finite difference algorithm implemented on a Cartesian mesh. Recently, more general finite volume algorithms have been introduced which are implemented on curvilinear body-conforming grids.[3] These recent developments have built upon the successful results of the major research effort which has been undertaken over the last 30 years in the area of computational fluid dynamics.

Unstructured-grid-based finite element methods have been the subject of much recent research activity in the area of computational aerodynamics.[4] The major attraction of the unstructured

CCC 0271–2091/94/210849–15
© 1994 by John Wiley & Sons, Ltd.
Received January 1994
Revised April 1994

grid approach is its geometrical flexibility and the availability of automatic unstructured mesh generators which can handle routinely computational domains of arbitrary geometric complexity.[5,6] These benefits of the unstructured approach will be of equal importance in the area of computational electromagnetics, but they can only be accessed if unstructured grid solution algorithms are developed for Maxwell's equations.[7,8]

In this paper we describe how an unstructured grid finite solver for the compressible Euler equations[9] can be modified to deal with electromagnetic scattering problems. The performance of the resulting procedure is demonstrated by application to a number of problems in both two and three dimensions.

2. MAXWELL'S EQUATIONS

Maxwell's equations governing the propagation of electromagnetic waves in free space are considered in the form

$$\varepsilon_0 \frac{\partial \mathbf{E}^*}{\partial t} = \text{curl } \mathbf{H}^*, \tag{1}$$

$$\mu_0 \frac{\partial \mathbf{H}^*}{\partial t} = -\text{curl } \mathbf{E}^*. \tag{2}$$

Here $\mathbf{E}^* = (E_1^*, E_2^*, E_3^*)$ and $\mathbf{H}^* = (H_1^*, H_2^*, H_3^*)$ denote the electric and magnetic field intensity vectors respectively, ε_0 is the dielectric permittivity and μ_0 is the magnetic permeability of free space. For the development of the solution algorithm it is convenient to observe that this pair of equations may be expressed alternatively in the conservation form

$$\frac{\partial \mathbf{U}^*}{\partial t} + \frac{\partial \mathbf{F}_j^*}{\partial x_j} = \mathbf{0}, \quad j = 1, 2, 3, \tag{3}$$

relative to a Cartesian co-ordinate system $Ox_1x_2x_3$, where the summation convention has been employed and where

$$\mathbf{U}^* = \begin{bmatrix} \mathbf{E}^* \\ \mathbf{H}^* \end{bmatrix}. \tag{4}$$

In this form the flux vectors are defined according to

$$\mathbf{F}_1^* = \begin{bmatrix} 0 \\ H_3^*/\varepsilon_0 \\ -H_2^*/\varepsilon_0 \\ 0 \\ -E_3^*/\mu_0 \\ E_2^*/\mu_0 \end{bmatrix}, \qquad \mathbf{F}_2^* = \begin{bmatrix} -H_3^*/\varepsilon_0 \\ 0 \\ H_1^*/\varepsilon_0 \\ E_3^*/\mu_0 \\ 0 \\ -E_1^*/\mu_0 \end{bmatrix}, \qquad \mathbf{F}_3^* = \begin{bmatrix} H_2^*/\varepsilon_0 \\ -H_1^*/\varepsilon_0 \\ 0 \\ -E_2^*/\mu_0 \\ E_1^*/\mu_0 \\ 0 \end{bmatrix}. \tag{5}$$

Considerable research effort has been expended recently into the development of accurate and efficient numerical techniques for the solution of problems involving compressible high-speed aerodynamic flows. For such problems the governing equations are generally considered in the conservation form of equation (3). The advantage of working with Maxwell's equations expressed in this form is that numerical techniques which have been developed for the solution of the

equations of compressible flows can then be applied, with minor modification, to the simulation of scattering problems.

For problems involving the scattering of electromagnetic waves by a perfectly conducting obstacle, the total fields $\mathbf{E}^*$ and $\mathbf{H}^*$ are regarded as being made up of incident and scattered components, i.e.

$$\mathbf{E}^* = \mathbf{E}_i + \mathbf{E}, \qquad \mathbf{H}^* = \mathbf{H}_i + \mathbf{H}. \tag{6}$$

The incident fields $\mathbf{E}_i$ and $\mathbf{H}_i$ satisfy the above equations and hence so do the scattered fields $\mathbf{E}$ and $\mathbf{H}$. The approach which is followed is then to solve equation (3) for the scattered field only.

3. THE NUMERICAL SCHEME

The algorithm which has been adopted to advance the solution in time is an explicit two-step finite-element-based Taylor–Galerkin procedure.[9] This is the finite element equivalent of the finite difference Lax–Wendroff method[10] and results in an algorithm which is notionally second-order-accurate in both time and space.

Discretization in time

To develop the scheme, we consider a Taylor expansion of the solution $\mathbf{U}(\mathbf{x}, t)$ in time in the form

$$\mathbf{U}^{n+1} = \mathbf{U}^n + \Delta t \left.\frac{\partial \mathbf{U}}{\partial t}\right|^n + \frac{\Delta t^2}{2} \left.\frac{\partial^2 \mathbf{U}}{\partial t^2}\right|^n, \tag{7}$$

where the superscript n denotes an evaluation at time $t = t_n$ and the time step $\Delta t = t_{n+1} - t_n$. This equation may be rewritten using the governing equation (3) to give the explicit time-stepping scheme

$$\Delta \mathbf{U} = -\Delta t \frac{\partial \mathbf{F}_j^n}{\partial x_j} + \frac{\Delta t^2}{2} \frac{\partial}{\partial x_j}\left(\mathbf{A}_j \frac{\partial \mathbf{F}_k}{\partial x_k}\right)^n, \tag{8}$$

where

$$\Delta \mathbf{U} = \mathbf{U}^{n+1} - \mathbf{U}^n, \qquad \mathbf{A}_j = \frac{\mathrm{d}\mathbf{F}_j}{\mathrm{d}\mathbf{U}}. \tag{9}$$

If the approximation

$$\mathbf{F}_j^{n+1/2} = \mathbf{F}_j^n - \frac{\Delta t}{2}\left(\mathbf{A}_j \frac{\partial \mathbf{F}_k}{\partial x_k}\right)^n \tag{10}$$

is employed, equation (8) may be written as

$$\Delta \mathbf{U} = -\Delta t \frac{\partial \mathbf{F}_j^{n+1/2}}{\partial x_j}. \tag{11}$$

Thus, if an initial approximation to $\mathbf{U}^{n+1/2}$ is determined from

$$\mathbf{U}^{n+1/2} = \mathbf{U}^n + \frac{\Delta t}{2} \left.\frac{\partial \mathbf{U}}{\partial t}\right|^n = \mathbf{U}^n - \frac{\Delta t}{2} \frac{\partial \mathbf{F}_j^n}{\partial x_j} \tag{12}$$

and equation (11) is then used to determine the increment $\Delta\mathbf{U}$, the result is a two-step procedure for advancing the solution in time which does not involve the Jacobian matrices $\mathbf{A}_j$. In practice, following the spatial discretization of the domain, this process is performed using the Galerkin approximation procedure.[11]

Discretization in space

The computational domain Ω is represented by an unstructured assembly of either linear three-noded triangular elements of four-noded tetrahedral elements. The discretization of the computational domain is accomplished by the use of an advancing front mesh generation method.[5] Piecewise linear approximations are employed for the increment $\Delta\mathbf{U}$, the solution $\mathbf{U}^n$ and the fluxes $\mathbf{F}_j^n$ in the form

$$\Delta\mathbf{U} \approx \Delta\hat{\mathbf{U}}^n = N_J \Delta\mathbf{U}_J, \qquad \mathbf{U} = N_J \mathbf{U}_J^n, \qquad \mathbf{F}_j^n \approx \hat{\mathbf{F}}_j^n = N_J \mathbf{F}_{jJ}^n, \tag{13}$$

where N_J denotes the linear finite element shape function associated with node J of the mesh. The functions $\mathbf{U}^{n+1/2}$ and $\mathbf{F}_j^{n+1/2}$ are represented in a piecewise linear discontinuous fashion, which means that for each element e in the mesh

$$\mathbf{U}^{n+1/2} \approx \hat{\mathbf{U}}^{n+1/2} = \mathbf{U}^n - \frac{\Delta t}{2} \frac{\partial N_J}{\partial x_j} \mathbf{F}_{jJ}^n, \qquad \mathbf{F}_j^{n+1/2} \approx \hat{\mathbf{F}}_j^{n+1/2} = N_J \mathbf{F}_{jJ}^{n+1/2}, \tag{14}$$

where the summations over the subscript J in equation (14) are taken only over the nodes belonging to element e. These quantities are therefore determined directly for each element in turn and equation (11) is then approximately satisfied via a Galerkin statement. The resulting system of equations may be written as

$$\mathbf{M}\delta\mathbf{U} = \mathbf{R}, \tag{15}$$

where typical entries in the matrices appearing here are defined by

$$\mathbf{M}_{JK} = \int_\Omega N_J N_K \, \mathrm{d}\Omega, \quad \delta\mathbf{U}_K = \Delta\mathbf{U}_K, \qquad \mathbf{R}_J = -\Delta t \left(\int_\Gamma n_j \hat{\mathbf{F}}_j^{n+1/2} N_J \, \mathrm{d}\Gamma - \int_\Omega \hat{\mathbf{F}}_j^{n+1/2} \frac{\partial N_J}{\partial x_j} \, \mathrm{d}\Omega \right). \tag{16}$$

In the derivation of the expression for $\mathbf{R}_J$, the divergence theorem has been applied and $\mathbf{n} = (n_1, n_2, n_3)$ denotes the unit outward normal to the boundary Γ of Ω. For the computations which have been performed to date, the explicit character of the scheme has been maintained by replacing the standard consistent mass matrix $\mathbf{M}$ by its lumped (diagonal) equivalent.

The electromagnetic waves are propagated with a speed $1/\sqrt{(\varepsilon_0 \mu_0)}$ and this explicit scheme will be stable provided that a standard CFL-type condition is satisfied.[10] The allowable time step for the stability of the above scheme is determined by initially sweeping through each element e of the mesh in turn and computing

$$\Delta t = \min_e [\sqrt{(\varepsilon_0 \mu_0)} h_e], \tag{17}$$

where h_e denotes the minimum height of element e.

Single-frequency incident waves of the form

$$\mathbf{U} = \mathbf{U}_0 \mathrm{e}^{j(\omega t - \beta x_1)} \tag{18}$$

are considered, where $\mathbf{U}_0$ is a constant and $j = \sqrt{(-1)}$. The solution is advanced in time through a prescribed number of cycles until 'steady' conditions are achieved. A further cycle is then computed, during which time the solution at each node in the mesh is monitored to determine the amplitudes and phases of the components of the scattered electric and magnetic fields.

Boundary conditions

When solving for the scattered fields, correct scattered field boundary conditions need to be imposed at the surface of the scatterer. When the scatterer is a perfect conductor, the boundary conditions require that the tangential component of the total electric field and the normal component of the total magnetic field should both be zero at the surface. This implies that at the scatterer the scattered field components must satisfy the conditions

$$\mathbf{n} \times \mathbf{E} = -\mathbf{n} \times \mathbf{E}_i, \qquad \mathbf{n} \cdot \mathbf{H} = -\mathbf{n} \cdot \mathbf{H}_i, \tag{19}$$

where $\mathbf{n}$ denotes the unit normal vector to the surface.

In the scattering simulations which will be considered here, the infinite region surrounding the scatterer will be represented by a finite computational domain. The correct boundary condition which should be imposed at the outer computational boundary is then that the scattered field consists of only outgoing waves. In an attempt to prevent any wave reflection at this boundary, this condition is achieved by a simple filtering technique[12] which involves the explicit addition of diffusion[13] to the governing equations in the vicinity of the outer boundary.

4. THE COMPUTATION OF THE RCS

Far-field scattering data can be obtained from the results of the time domain computation by employing a near-field to far-field transformation. This procedure is outlined here for the three-dimensional case, but the two-dimensional situation can be handled in a similar fashion. We consider an arbitrary surface S which completely encloses the scatterer and employ the surface equivalence theorem[14] to set up an equivalent problem in the region external to S.

The solution computed by the time domain solver is used to determine the distribution of the scattered fields $\mathbf{E}$ and $\mathbf{H}$ on the surface S. These fields are then employed to obtain equivalent surface electric and magnetic currents $\mathbf{J}$ and $\mathbf{M}$ respectively on S according to

$$\mathbf{J} = \mathbf{n} \times \mathbf{H}, \qquad \mathbf{M} = -\mathbf{n} \times \mathbf{E}, \tag{20}$$

where $\mathbf{n}$ now denotes the unit outward normal vector to S.

Removing the time-harmonic component, the corresponding vector potentials $\mathbf{A}$ and $\mathbf{F}$ at any point $\mathbf{x} = (x_1, x_2, x_3)$ outside S can be obtained in the form

$$\begin{bmatrix} \mathbf{A} \\ \mathbf{F} \end{bmatrix} = \frac{1}{4\pi} \int_S \begin{bmatrix} \mu_0 \mathbf{J}(x') \\ \varepsilon_0 \mathbf{M}(\mathbf{x}') \end{bmatrix} \frac{e^{-j\beta R}}{R} \, dS, \tag{21}$$

where

$$R^2 = (x_1 - x_1')^2 + (x_2 - x_2')^2 + (x_3 - x_3')^2 \tag{22}$$

denotes the square of the distance from the point $\mathbf{x}' = (x_1', x_2', x_3')$ on S to the point $\mathbf{x}$. If the

co-ordinates (x_1, x_2, x_3) are expressed in terms of spherical polar co-ordinates (r, θ, ϕ), the far-field forms of these relations become apparent as

$$\begin{bmatrix} \mathbf{A} \\ \mathbf{F} \end{bmatrix} = -\frac{e^{-j\beta r}}{4} \int_S \begin{bmatrix} \mu_0 \mathbf{J}(\mathbf{x}') \\ \varepsilon_0 \mathbf{M}(\mathbf{x}') \end{bmatrix} e^{j\beta r^*} \, dS, \tag{23}$$

where

$$r^* = x'_1 \sin\theta \cos\phi + x'_2 \sin\theta \sin\phi + x'_3 \cos\theta, \tag{24}$$

and the corresponding far-field components of the scattered electric field can be determined in spherical polar form as

$$E_r \approx 0, \qquad E_\theta \approx -j\beta\eta A_\theta - j\beta F_\phi, \qquad E_\phi \approx -j\beta\eta A_\phi + j\beta F_\theta. \tag{25}$$

Here

$$\eta = \sqrt{\left(\frac{\mu_0}{\varepsilon_0}\right)} \tag{26}$$

and

$$A_\theta = A_1 \cos\theta \cos\phi + A_2 \cos\theta \sin\phi - A_3 \sin\theta, \qquad A_\phi = -A_1 \sin\phi + A_2 \cos\phi, \tag{27}$$

with similar expressions for F_θ and F_ϕ. The radar cross-section σ is computed as

$$\sigma = \lim_{r \to \infty} \left[4\pi r^2 \left(\frac{E_\theta^2 + E_\phi^2}{E_{i\theta}^2 + E_{i\phi}^2} \right) \right] \tag{28}$$

and the computational implementation outputs the quantity RCS which is defined by

$$\text{RCS} = 10 \log_{10}(\sigma). \tag{29}$$

It should be noted that in the computations which are presented below, the surface S is chosen to coincide exactly with the surface of the scatterer.

5. NUMERICAL EXAMPLES

Scattering by a circular cylinder

The first computations involve the simulation of the scattering of plane TE and TM waves by an infinite circular cylinder. These examples can be used for code validation, since analytical solutions are available.[14] For both polarizations the chosen incident wave is such that $\beta L = 3\pi$, where L is the cylinder radius. A detail of the computational domain and the mesh employed for the TE simulation are shown in Figure 1(a). The mesh consists of 68,612 elements and 34,632 nodes. A detail of the computed contours of the scattered H_3-field is given in Figure 1(b). The exact and numerically determined distributions of the RCS values are compared in Figure 1(c).

The TM simulation is undertaken on a coarser grid consisting of 39,584 elements and 20,085 nodes. A detail of the computed contours of the scattered E_3-field is shown in Figure 2(a). The exact and numerically determined distributions of the RCS values are compared in Figure 2(b).

Scattering by an NACA 0012 aerofoil

The simultation of the scattering of a plane TE wave by an NACA 0012 aerofoil is computed for the case $\beta L = 2\pi$, where L is now the chord length of the aerofoil. The mesh consists of 51,316 elements and 25,886 nodes and a detail of this mesh in the vicinity of the aerofoil is shown in Figure 3(a). The computed amplitude of the scattered H_3-field is displayed in Figure 3(b). The predicted RCS distribution is given in Figure 3(c).

Scattering by a semi-open cavity

This configuration is also of interest to the aerospace industry since it can be regarded as an idealized closed air intake. Geometrically, the configuration consists of two parallel walls which are connected at the right-hand end. This produces a semi-open cavity in the shape of a letter U rotated by 90°. The thickness of the walls is denoted by t and the outer dimensions are given by $a + t$ and $b + 2t$. This implies that the inner cavity has dimensions a and b. The simulation involves the scattering of a plane TE wave for which $\beta L = 2\pi$ by a cavity for which

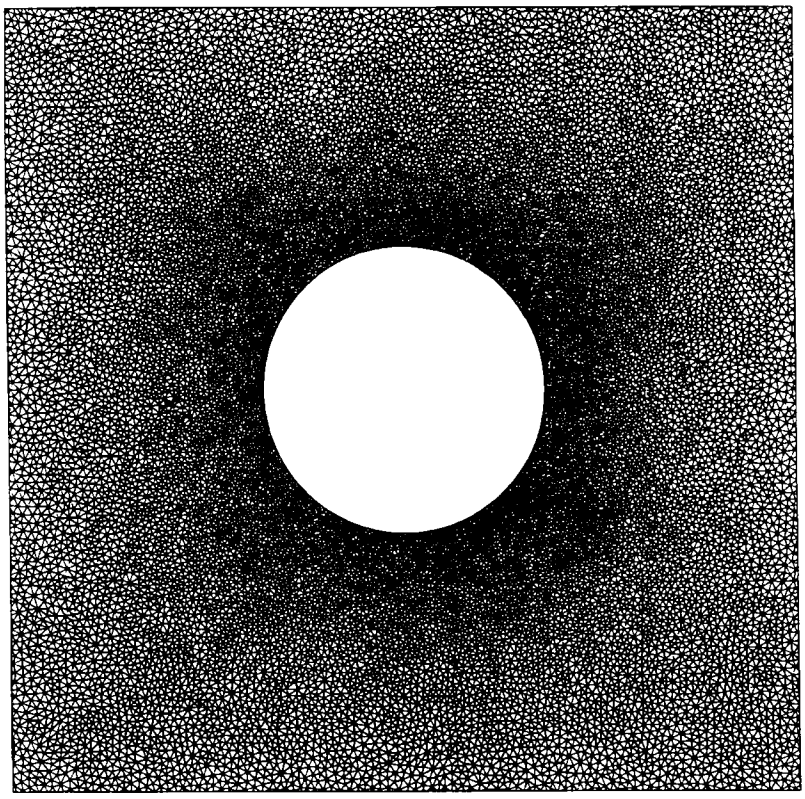

(a)

Figure 1. Scattering of a plane TE wave by a circular cylinder: (a) detail of the computational domain and the mesh employed; (b) detail of the computed contours of the scattered H_3-field; (c) comparison between the distribution of the exact and the computed RCS

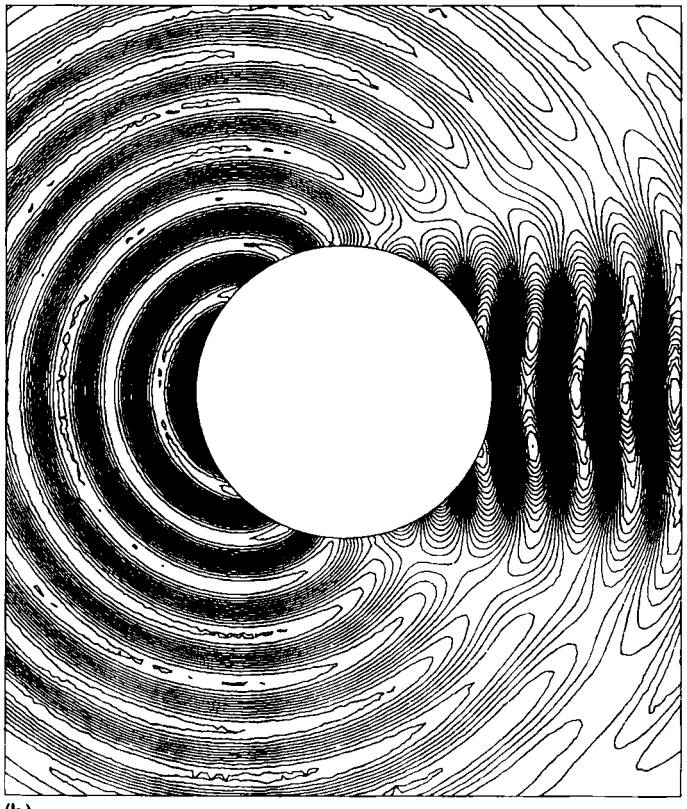

(b)

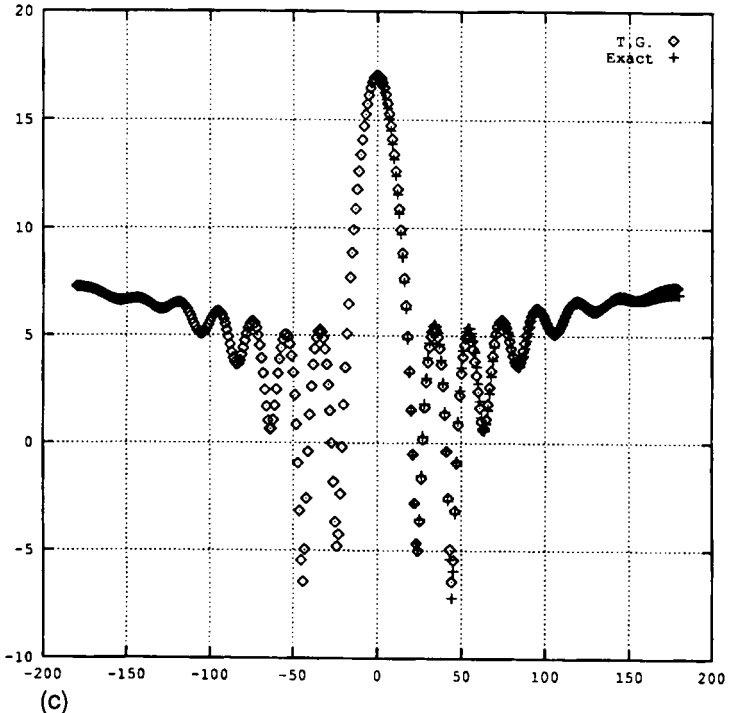

(c)

Figure 1. (*continued*)

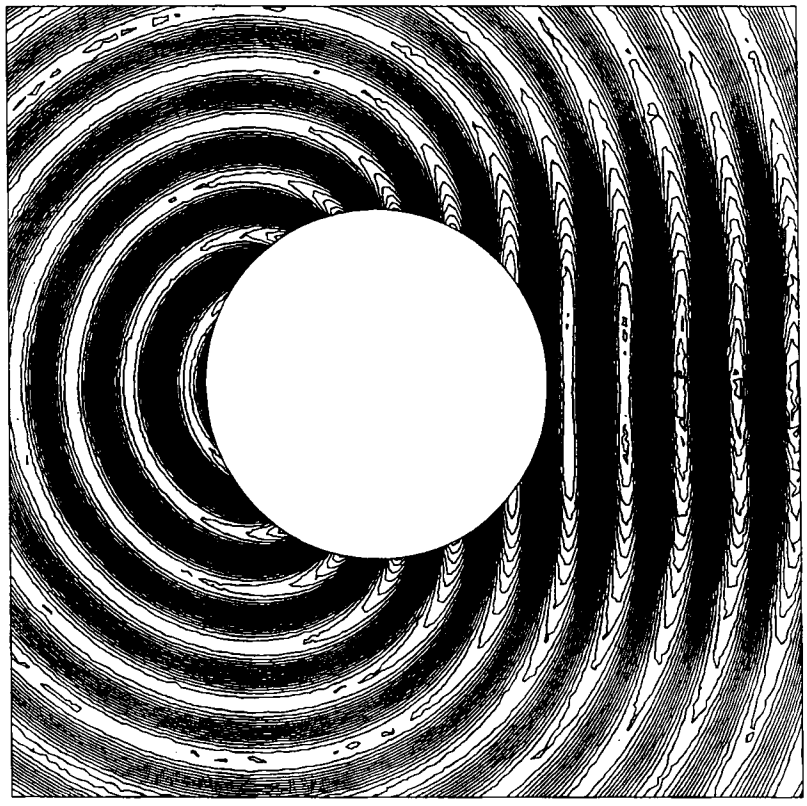

(a)

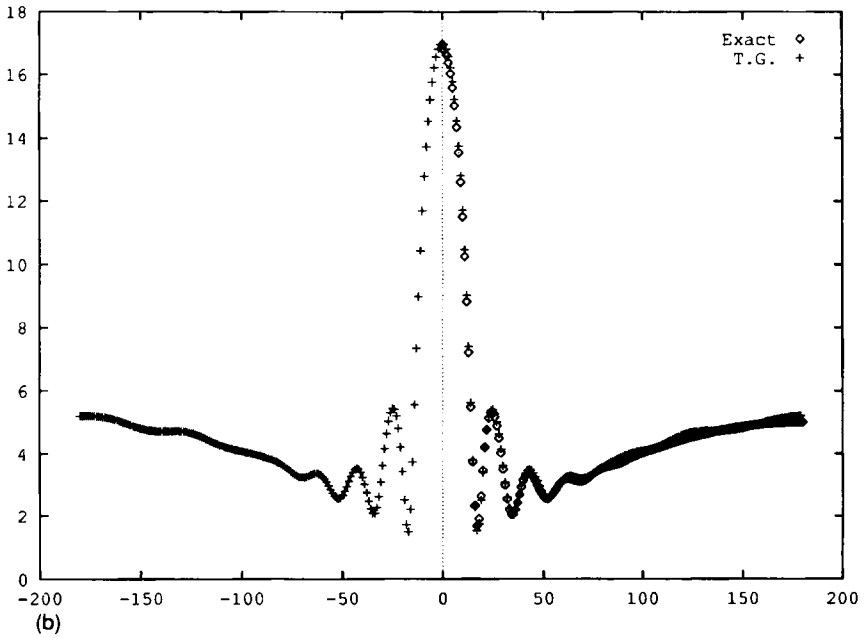

(b)

Figure 2. Scattering of a plane TM wave by a circular cylinder: (a) detail of the computed contours of the scattered E_3-field; (b) comparison between the distribution of the exact and the computed RCS

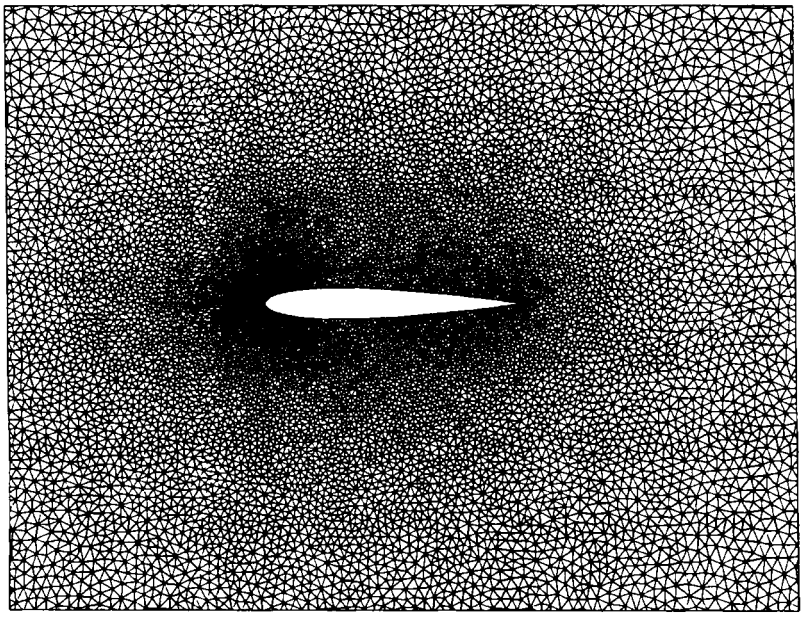

(a)

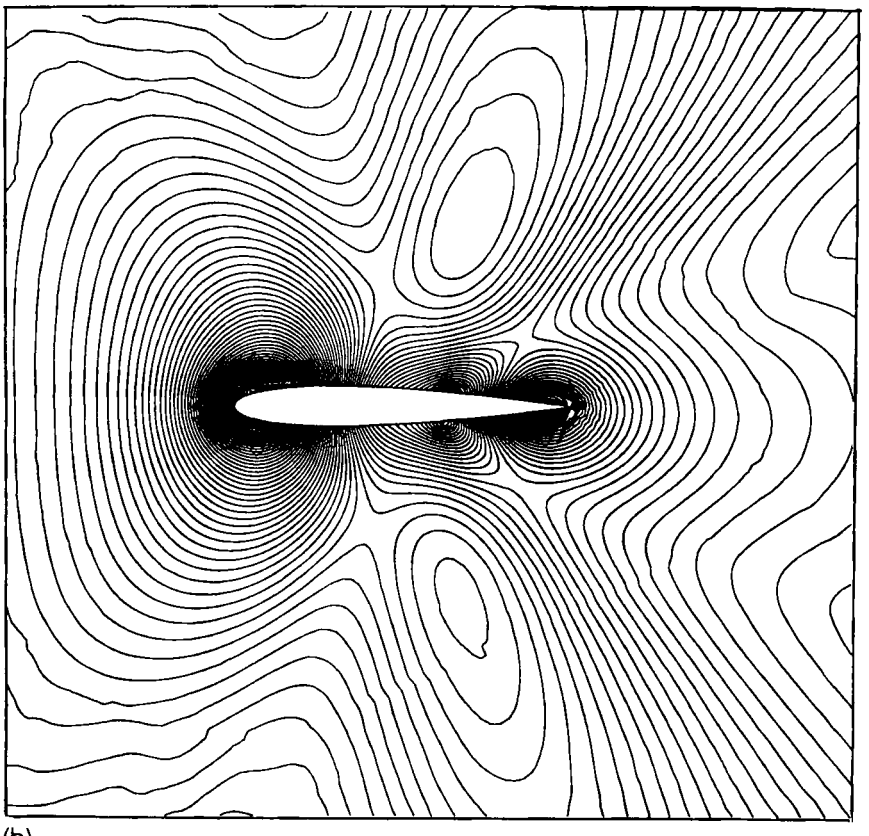

(b)

Figure 3. Scattering of a plane TE wave by an NACA 0012 aerofoil: (a) detail of the mesh employed; (b) computed contours of the amplitude of the scattered H_3-field; (c) distribution of the computed RCS

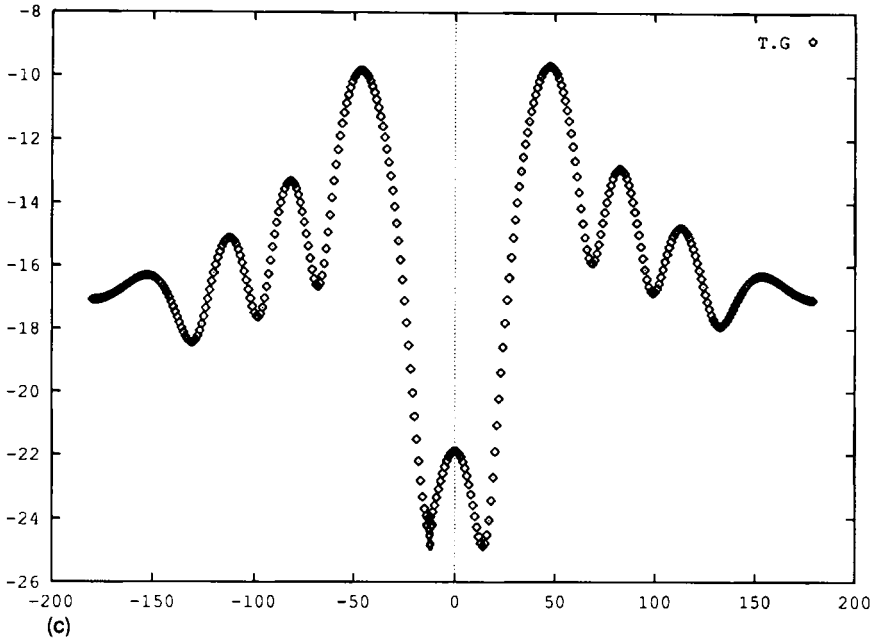

Figure 3 (*continued*)

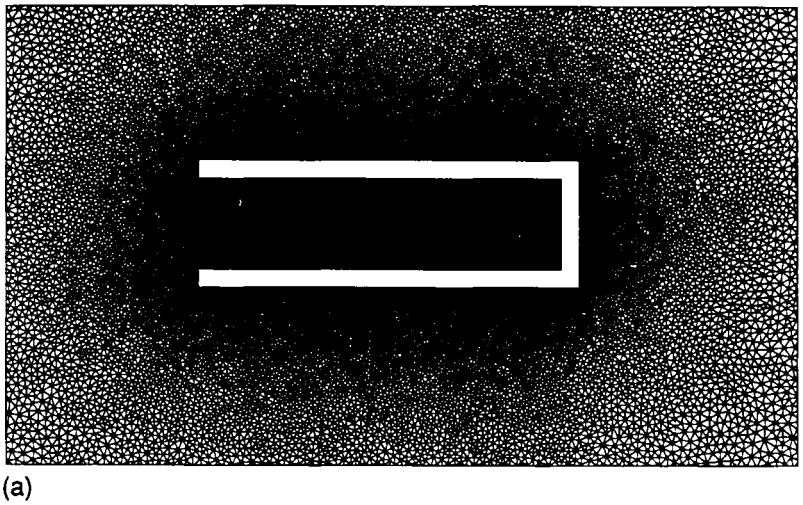

Figure 4. Scattering of a plane TE wave by a semi-open cavity: (a) detail of the mesh employed; (b) computed contours of the total H_3-field; (c) distribution of the computed RCS

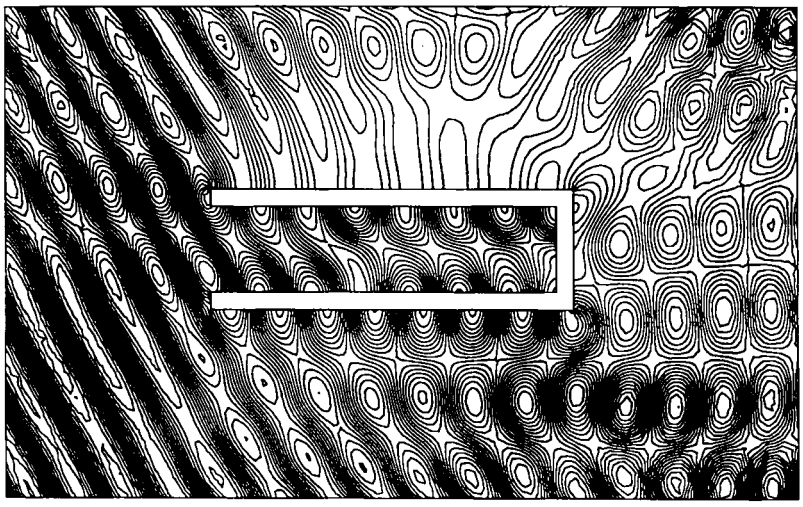

(b)

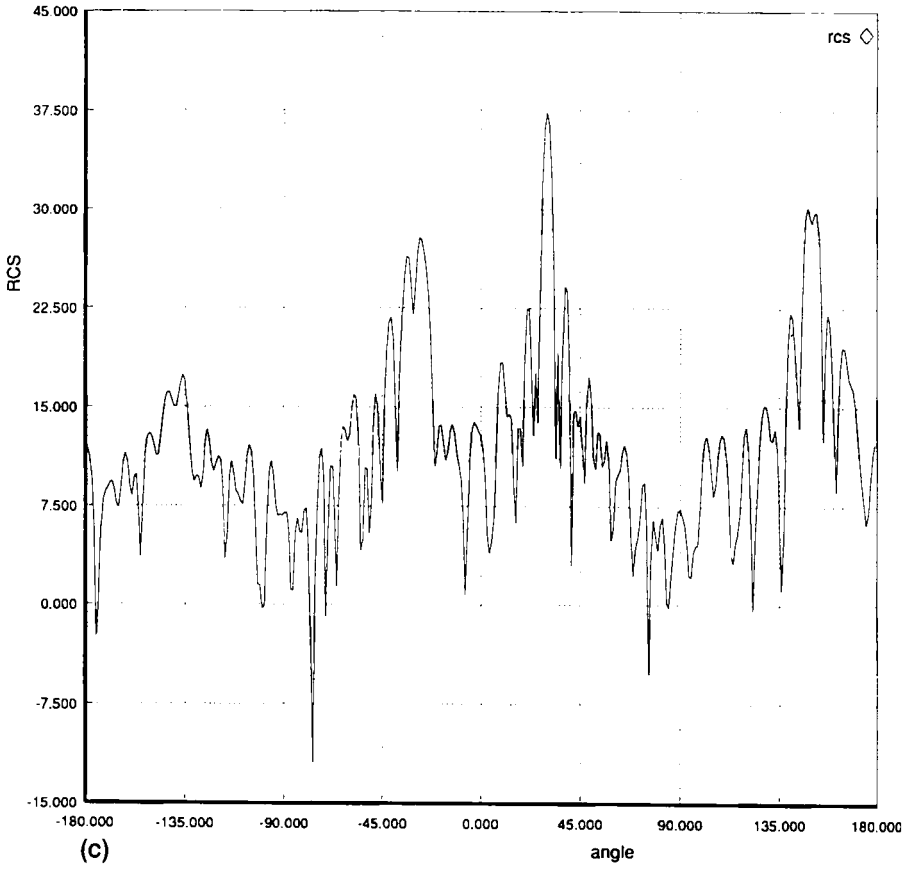

(c)

Figure 4 (*continued*)

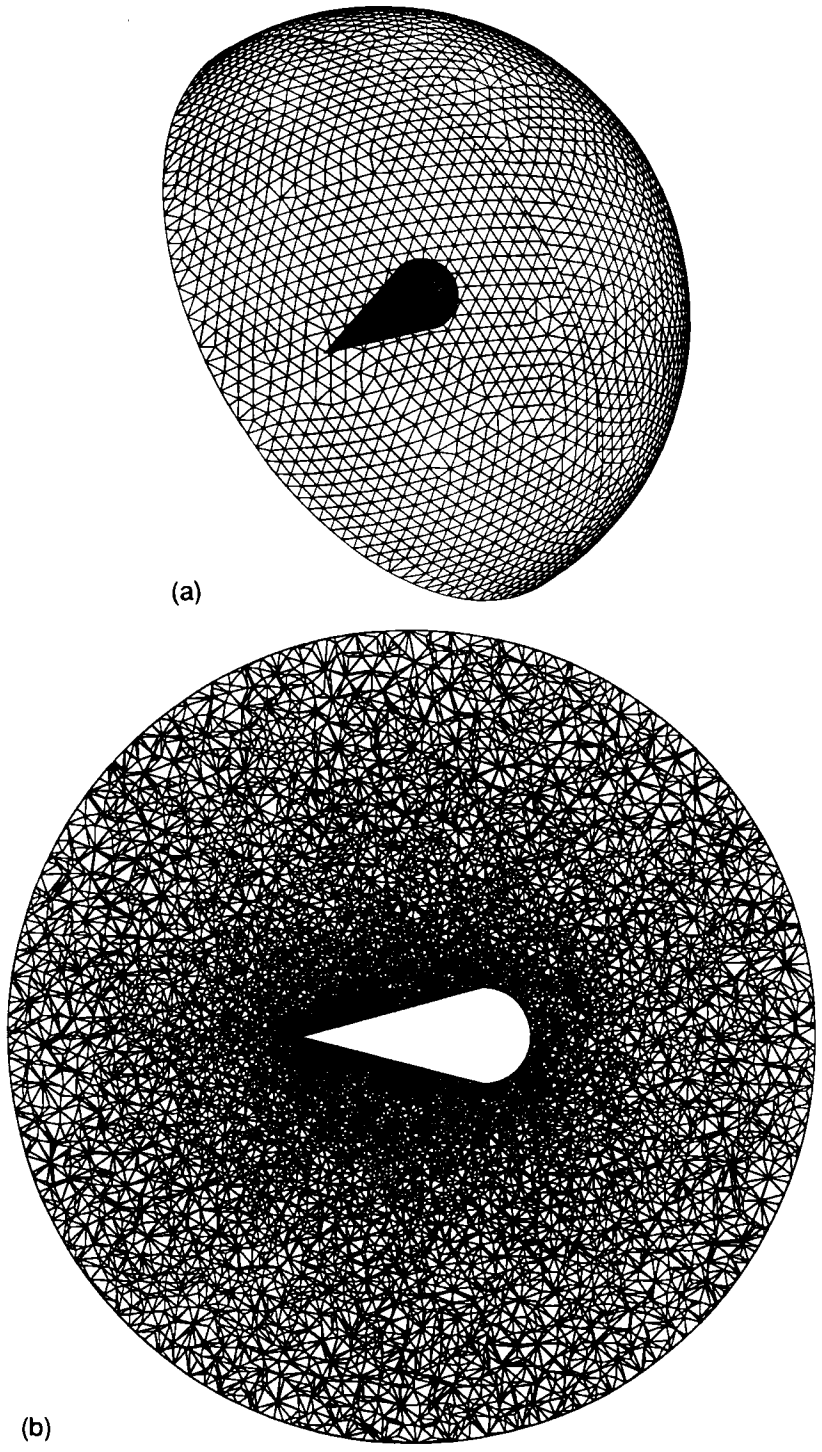

Figure 5. Scattering of a plane wave by a cone sphere: (a) partial view of the triangulation of the boundaries of the computational domain; (b) a cut through the complete volume mesh; (c) the scattered E-field vectors on the surface of the cone sphere

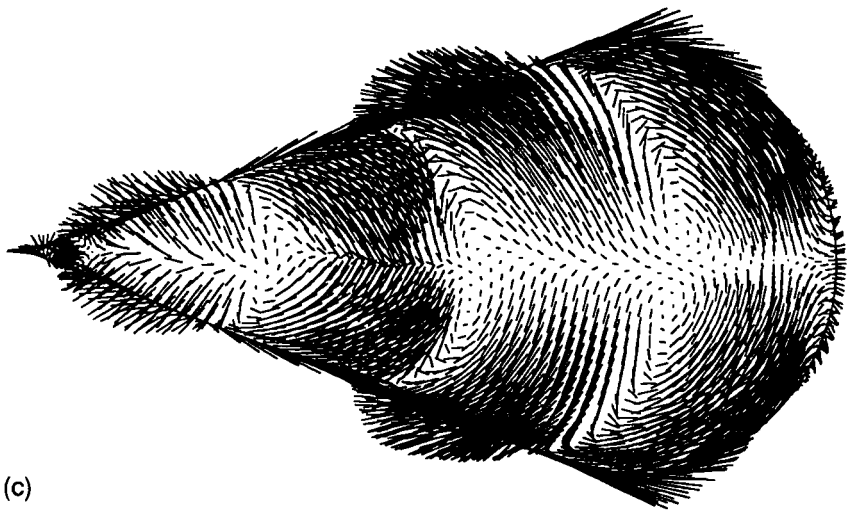

(c)

Figure 5 (*continued*)

$a = 4L$, $\beta = L$ and $t = 0.2L$, with the incident wave propagating in a direction which lies at an angle of 30° to the axis of the cavity. The mesh employed consists of 47,645 elements and 24,461 nodes and a detail of the mesh is shown in Figure 4(a). The computed contours of the total H_3-field are shown in Figure 4(b). The predicted RCS distribution is given in Figure 4(c).

These two-dimensional computations were performed interactively on the SERC CRAY YMP at the Rutherford Appleton Laboratory. Colouring[15] of the elements in the mesh ensures that the computer code can be vectorized and a highly efficient computational procedure results. The typical memory requirements are around 1.5 Mwords for a mesh of 50,000 triangular elements and run times of the order of 10 min were required to perform 800 time steps.

Scattering by a cone sphere configuration

To illustrate the 3D capability of the proposed procedure, we consider the simulation of the scattering of a plane wave by a cone sphere configuration. The incident wave is such that $\beta L = 3{\cdot}864\pi$ and $\beta R = \pi$, where L is the height of the cone and R is the radius of the sphere. The mesh employed consists of 664,114 tetrahedral elements and 105,938 nodes. A partial view of the triangulation of the computational boundary is shown in Figure 5(a), while Figure 5(b) gives an indication of the mesh density by showing a cut taken through the complete volume mesh. The solution is advanced for 5 cycles and the corresponding form of the scattered E-field on the surface of the cone sphere is indicated in Figure 5(c).

6. CONCLUSIONS

A time domain solver for the solution of the Maxwell equations on general unstructured triangular and tetrahedral meshes has been developed. In its present form the code provides an initial capability for the efficient simulation of electromagnetic scattering by perfectly conducting 2D and 3D bodies of general shape. Future work with this solver will concentrate upon full validation of the 3D capability and the incorporation of multi-material modelling. Recent

developments[16] in improving the efficiency and accuracy of unstructured mesh solvers for computational fluid dynamics will also need to be considered in the context of computational electromagnetics.

ACKNOWLEDGEMENTS

The authors acknowledge the support for this work provided by the Department of Computational Engineering, Sowerby Research Centre, British Aerospace plc. The two-dimensional computations were performed using computer time provided by the UK Science and Engineering Research Council under Research Grant GR/G 59240.

REFERENCES

1. A. Taflove, 'Re-inventing electromagnetics: supercomputing solution of Maxwell's equations via direct time integration on space grids', *AIAA Paper 92-0333*, 1992.
2. K. S. Yee, 'Numerical solution of initial boundary value problems involving Maxwell's equations in isotropic media', *IEEE Trans. Antennas Propagat.*, **AP-14**, 302–307 (1966).
3. V. Shankar, W. F. Hall, A. Mohammadian and C. Rowell, 'Algorithmic aspects and superconduting trends in computational electromagnetics', *AIAA Paper 93-0367*, 1993.
4. K. Morgan, J. Peraire and J. Peiró, 'Unstructured grid methods for compressible flows', in *AGARD Rep. R-787: Unstructured Grid Methods for Advection Dominated Flows*, AGARD, Paris, 1992, pp. 5.1–5.39.
5. J. Peraire, M. Vahdati, K. Morgan and O. C. Zienkiewicz, 'Adaptive remeshing for compressible flow computations', *J. Comput. Phys.*, **72**, 449–466 (1987).
6. N. P. Weatherill, 'The Delaunay triangulation in computational fluid dynamics', *Comput. Math. Appl.*, **24**, 129–150 (1992).
7. B. Petitjean and R. Löhner, 'Finite element solvers for radar cross-section (RCS) calculations', *AIAA Paper 92-0455*, 1992.
8. J. P. Cioni, L. Fezoui and H. Steve, 'A parallel time-domain Maxwell solver using upwind schemes and triangular meshes', *IMPACT in Computing in Science and Engineering 165*, 1993.
9. K. Morgan, J. Peraire, J. Peiró and O. Hassan, 'The computation of three dimensional flows using unstructured grids', *Comput. Methods Appl. Mech. Eng.*, **87**, 335–352 (1991).
10. C. Hirsch, *Numerical Computation of Internal and External Flows*, Vols 1 and 2, Wiley, Chichester, 1988.
11. O. C. Zienkiewicz and K. Morgan, *Finite Elements and Approximation*, Wiley, Chichester, 1983.
12. D. Givoli, *Numerical Methods for Problems in Infinite Domains*, Elsevier, Amsterdam, 1992.
13. J. Peraire, K. Morgan, J. Peiró and O. C. Zienkiewicz, 'An adaptive finite element method for high speed flows', *AIAA Paper 87-0559*, 1987.
14. C. A. Balanis, *Advanced Engineering Electromagnetics*, Wiley, Chichester, 1989.
15. L. Formagia, J. Peraire, K. Morgan and J. Peiró, 'Implementation of a 3D explicit Euler solver on a CRAY computer', *Proc. 4th Int. Symp. on Science and Engineering on CRAY Supercomputers*, CRAY Research, Minneapolis, MN, 1988, pp. 45–65.
16. J. Peraire, J. Peiró and K. Morgan, 'Finite element multigrid solution of Euler flows past installed aero-engines', *Comput. Mech.*, **11**, 433–451 (1993).